

JAAS

Accepted Manuscript



This is an *Accepted Manuscript*, which has been through the Royal Society of Chemistry peer review process and has been accepted for publication.

Accepted Manuscripts are published online shortly after acceptance, before technical editing, formatting and proof reading. Using this free service, authors can make their results available to the community, in citable form, before we publish the edited article. We will replace this *Accepted Manuscript* with the edited and formatted *Advance Article* as soon as it is available.

You can find more information about *Accepted Manuscripts* in the [Information for Authors](#).

Please note that technical editing may introduce minor changes to the text and/or graphics, which may alter content. The journal's standard [Terms & Conditions](#) and the [Ethical guidelines](#) still apply. In no event shall the Royal Society of Chemistry be held responsible for any errors or omissions in this *Accepted Manuscript* or any consequences arising from the use of any information it contains.

ARTICLE

Palaeolithic paint palette used at La Garma cave (Cantabria, Spain) investigated by means of combined *in situ* and synchrotron X-ray analytical methods

alfeCite this: DOI:
10.1039/x0xx00000x

Received 00th January 2012,
Accepted 00th January 2012

DOI: 10.1039/x0xx00000x

www.rsc.org/

M. Gay,^a M. Alfeld,^b M. Menu,^c E. Laval,^c P. Arias,^d R. Ontañón^d and I. Reiche^{a*}

La Garma cave is part of the most exceptional Palaeolithic sites discovered at the end of the 20th century in the North of the Spain and was included by UNESCO in the World Heritage List in 2008. This cave contains more than 500 exceptional Palaeolithic graphical units, some of them linked to the Magdalenian floors. The La Garma cave was never opened to the public and thus provides a closed karst system with untouched archaeological surfaces, conferring to it an important position in the study of the Upper Palaeolithic in this region. A combined analytical strategy was chosen to enhance the understanding of the rock art distribution in this cave, looking for different decorative steps. SEM-EDX analysis carried out on fifty-six samples was complemented by μ XRF and μ XANES measurements at the Fe K-edge at the Deutsches Elektronen-Synchrotron DESY (Hamburg, Germany). A systematic study of the prehistoric representations on-site has been initiated with portable XRF instruments. The new data acquired by the combination of synchrotron radiation methods and the first *in situ* measurements in the cave give more detailed insights into the characterisation of the pictorial matters used by the prehistoric artists. Data evaluation was performed using principal component analyses. It offers arguments to link specific pictorial properties to particular periods of ornamentation inside the cave.

Introduction

The Lower Gallery of La Garma is a major site of Palaeolithic rock art in the Cantabrian region, and one of the most relevant for the study of its archaeological context. The original entrance was blocked at the end of the Pleistocene and so the Upper Palaeolithic floors and structures were preserved in their original state. Hence, this site offers a rare state of preservation for rock art research. It contains an important ensemble of rock art including more than 500 graphic units, among them 92 animal figures, 109 signs and 40 hand stencils. On the basis of its importance, La Garma has been included in the World Heritage List of the UNESCO.

The Lower Gallery with its well preserved Magdalenian floors also provides exceptional information about the context in which the rock art was produced. Some stains of paint on the floor, palettes with remains of crushed iron oxide and the sources of certain raw materials used to prepare the paintings in the cave have been studied¹. The first physicochemical studies of this rock art were conducted in order to enhance the archaeological and stylistic knowledge acquired about the cave^{2,3,4,5}. This additional information complements that provided by archaeological investigations, by providing knowledge about the composition of the palettes used by prehistoric artists. This has improved the comprehension of the overall organisation of the figures inside this cave and allows highlighting the existence of different decorative steps.

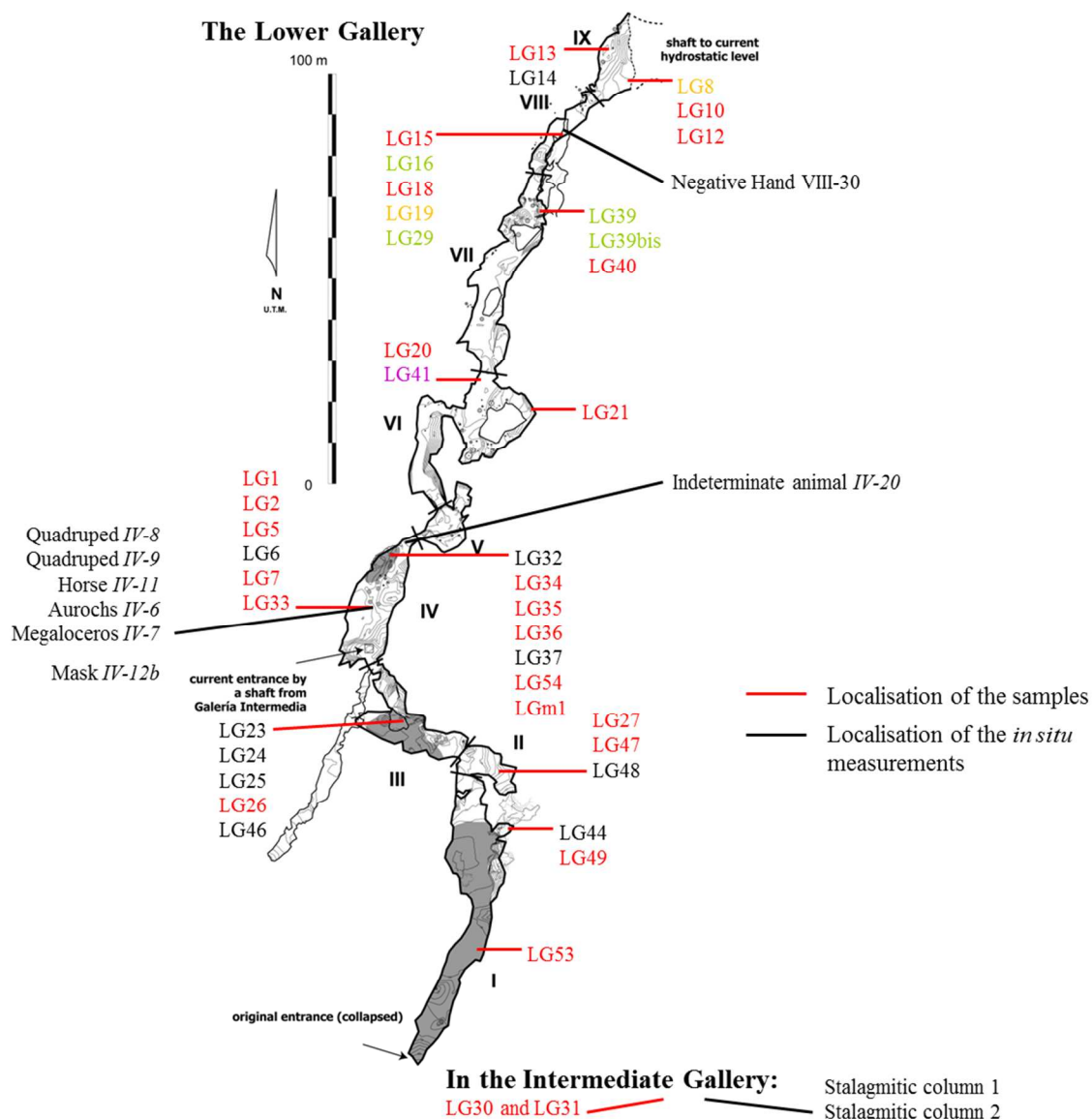


Fig1: Localisation of the 42 analysed samples by SEM-EDX among the 56 which were sampled in the Intermediate and Lower Galleries. Localisation of the figures analysed by pXRF in the Intermediate and Lower Galleries.

To achieve these new observations, 56 representative samples¹ of La Garma rock art have been first physicochemically characterised by energy dispersive X-ray spectrometry coupled to a scanning electron microscope (SEM-EDX) in the Centre for Research and Restoration of the French Museums (C2RMF) in Paris. The new results has answered many archaeological questions about the preparation of the paint matter and the use of specific paint pots, providing the basis for a better understanding of this major decorated cave. However, some issues remained unresolved, requiring complementary analyses by micro-X-ray fluorescence and micro-X-ray absorption near edge structure (μ XRF/ μ XANES) analyses of the Fe K-edge at beamline P06 of the Deutsches Elektronen-Synchrotron in Hamburg (Germany) to determine oxidation state and coordination environment.

Both methods, synchrotron X-ray and SEM-EDX analyses, are well-established techniques for the study of rock art^{6,7}. They are mainly focussed on the characterisation of the pigment and its physical properties and chemical composition. As they are destructive methods, they are limited to the investigation of samples taken from the original art works. In order to investigate a wider range of art works in La Garma cave while preserving the integrity of its prehistoric representations, *in situ* investigations were done with a mobile XRF instrument. The use of such portable methods is becoming more widespread^{8,9,10,11}, taking advantage of the instrumental developments made in the last few years in the XRF technique¹². This led to a renewal of the physicochemical analyses of rock art with non-invasive methods.

The question posed in this article is whether a specific palette (as chemically identified) can be linked to the ornamentation of

a particular room and/or to a specific decorative step. In investigating this question, we have gained detailed insights into the spatial, stylistic and temporal relationships between the figures.

Additionally, we address the extent to which the different methods used are complementary. Further, a procedure is presented to account for the effect of the wall support in the evaluation of the *in situ* measurements.

Materials

Archaeological material

Samples

In a previous study¹, 56 micro samples of pigments have been taken from the Intermediate and Lower galleries of La Garma (Fig1). In the order scale of just a few one-tenths of a millimetre, they have been carefully selected by Pablo Arias and co-workers in order to be representative of the different colours (black, red, yellow and purple) and decorated areas found in the cave. This set of samples gathered different mineral phases of iron oxides, manganese oxides, mixtures and charcoal. The selected samples therefore provide a global vision, as representative as possible, of the pictorial matter used by prehistoric artists at La Garma. They have been taken off with a sterile scalpel blade.

Twenty-six of the 56 micro-samples (from LG30 to LG55) previously observed and analysed by SEM-EDX have been recently the target of synchrotron μ XRF and μ XANES analyses.

Decorated panels

In parallel, non-invasive analyses have been performed in the cave using a portable X-ray fluorescence spectrometry (pXRF) instrument. Different decorated areas of interest were chosen for this first *in situ* study of the rock art of La Garma. In total, three zones have been analysed, as indicated in Fig1: two in the Lower Gallery, the zones IV and VIII, and one in the Intermediate Gallery. These areas are extremely difficult to access and require the use of portable instruments of minimal

possible weight. Therefore, a series of spots was investigated, but no imaging experiments were done. However, the non-invasive nature of such instruments enables the acquisition of statistically relevant data by multiple measurements of different spots on the same artistic element, as it is illustrated by the example of two decorated panels (Fig2). With a particular attention, each analysed point had to be representative for the investigated figure. In total, 57 points from ten individual representations and one stain of red pictorial matter were measured (Table1). In all cases, the underlying rock surface was analysed for comparison.

Reference compounds for XANES

Based on the work of Wilke *et al.*¹³, four compounds have been selected for the characterisation of Fe^{2+} and Fe^{3+} in the various coordination environments: Siderite ($\text{Fe}^{2+}\text{CO}_3$) and Staurolite ($\text{Fe}^{2+}_4\text{Al}_{18}\text{Si}_8\text{O}_{46}(\text{OH})_2$) for $^{\text{VI}}\text{Fe}^{2+}$ and $^{\text{IV}}\text{Fe}^{2+}$, respectively, and Andradite ($\text{Ca}_3\text{Fe}^{3+}_2(\text{SiO}_4)_3$) and Ferriorthoclase ($\text{Fe}^{3+}\text{PO}_4$) for $^{\text{VI}}\text{Fe}^{3+}$ and $^{\text{IV}}\text{Fe}^{3+}$, respectively. The reference compounds were pressed into pellets with boron nitride.

Experimental

Synchrotron instrumentation

Scanning μ XRF and μ XANES measurements at the Fe K-edge were performed at the Hard X-ray Microprobe beamline P06 at the PETRA III storage ring of the Deutsches Elektronen-Synchrotron (DESY).

The primary radiation emitted by the undulator device was monochromatized with an Oxford High-heat load Double-crystal Monochromator using Si (111) crystals and focused by a pair of KB-mirrors, yielding a beam size of $0.6 \times 0.6 \mu\text{m}^2$.

The intensity of the primary beam before the sample was recorded with an ionization chamber, while the intensity of the transmitted beam was determined with a PIPS diode. The fluorescence radiation emitted by the sample was recorded with a Maia detector array, which consists of 384 energy dispersive detector elements with an active area of 1 mm^2 each. The Maia detector is designed for fast imaging experiments and provides

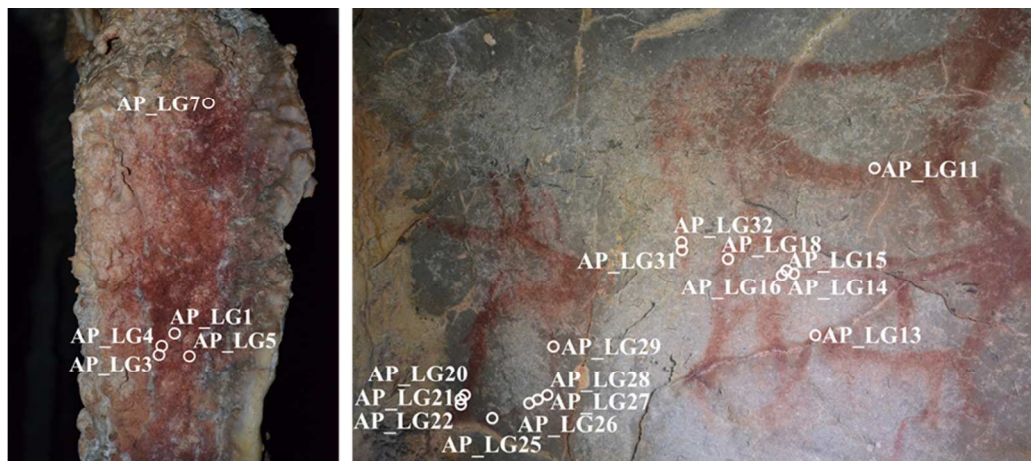


Fig2: Indication of the analysed points in the stalagmitic column 1 (Intermediate Gallery) and in the decorated panel of the southern part of the zone IV (Lower Gallery), which includes five animal representations (aurochs IV-6, megaloceros IV-7, quadrupeds IV-8 and IV-9 and horse IV-11).

Reference	Prehistoric representation	Localisation	Colour	Number of XRF measurements	Previous SEM-EDX result ¹
AP_LG1 AP_LG3 AP_LG4 AP_LG5 AP_LG7	Stalagmitic column 1	Intermediate Gallery	Red	n=5	Hematite Hb0.1
AP_LG9	Stalagmitic column 2	Intermediate Gallery	Red	n=1	Hematite Hb0.1
AP_LG20 AP_LG21 AP_LG22	Aurochs IV-6	Zone IV, Lower Gallery	Red	n=3	Hematite Hb0.5
AP_LG25 AP_LG26 AP_LG27 AP_LG28 AP_LG29	Megaloceros IV-7	Zone IV, Lower Gallery	Red	n=2	Hematite Hp5
AP_LG11 AP_LG31 AP_LG32	Quadruped IV-8	Zone IV, Lower Gallery	Red	n=3	Non-analysed
AP_LG13 AP_LG18	Quadruped IV-9	Zone IV, Lower Gallery	Red	n=2	Hematite Hp5
AP_LG14 AP_LG15 AP_LG16	Horse IV-11	Zone IV, Lower Gallery	Red	n=3	Hematite Hp5
AP_LG34 AP_LG35 AP_LG36	Mask IV-12b	Zone IV, Lower Gallery	Red	n=3	Hematite Hp5
AP_LG37 AP_LG38 AP_LG39			Black	n=3	Manganese oxide
AP_LG44 AP_LG45 AP_LG47	Indeterminate animal IV-20	Zone IV, Lower Gallery	Black	n=3	Manganese oxide
AP_LG50 AP_LG51			Red stain	n=2	Non-analysed
AP_LG54 AP_LG55	Negative Hand VIII-30	Zone VIII, Lower Gallery	Yellow	n=2	Non-analysed

Table 1: Description of selected area and representations analysed by XRF spectrometry. Related with previous SEM-EDX results.

outgoing count rates of up to 10 Million counts per second. Consequently, it allows acquiring elemental distribution images with a dwell time below 1 ms¹⁴, provided the elements of interest in the sample give rise to fluorescence radiation of sufficient intensity.

For the investigation at beamline P06, 26 selected samples from La Garma cave were deposited in powdered form on Mylar® tape, which was mounted on a same sample carrier. An overview scan of the entire range of samples was done with a step size of 5 µm and a dwell time of 1 ms at a primary energy of 21.2 keV.

The primary energy was lowered after this scan to 7.2 keV for the acquisition of XANES data. XANES acquisition was

performed in imaging mode, i.e. a stack of elemental distribution images is acquired at different primary energies. After fitting the raw data the result is a data cube with two lateral dimensions and one energy dimension, in which a full XANES spectrum is acquired for each pixel investigated.

The XANES profiles were recorded in the energy range of 7.08-7.20 keV, with an energy step size of 0.5 eV, with the exception of the pre-edge range (7.106-7.118 keV), in which an energy step of 0.1 eV was used, and the energy range from 7.14 to 7.20 keV, for which an energy step of 1.0 eV was used.

Reference XANES profiles were acquired on reference samples under the same conditions as given above. Meaningful profiles

were acquired by summing the XANES scans of several hundred pixels per material.

The samples were measured in a similar fashion with a lateral step size 50 μm and 1 ms dwell time. The rather coarse lateral resolution and the dwell time were due to technical difficulties of the storage ring, which reduced the time available for the experiment. The data evaluation was performed with the GeoPIXE software package¹⁵.

***In situ* instrumentation and data evaluation**

The XRF analyses have been carried out with a portable spectrometer constructed in-house. This device is composed of a 40 kV MOXTEK X-ray tube with a palladium anode. By employing a collimator, a beam spot size of approximately 1mm² on the sample is achieved. The XRF signal is collected by a 7 mm² Silicon Drift Detector with an energy resolution of 140 eV (FWHM at 5.9 keV). The incident angle of the X-ray is 45° to the analysed surface while the detector is perpendicular to it. Both X-ray tube and detector are fixed on a positioning system allowing micrometric movements that is itself fixed on a tripod (Fig3). This configuration is well-suited for the study of panels that are difficult to access.



Fig3: Portable XRF apparatus implemented in La Garma cave.

Semi-quantitative data obtained by XRF have been extracted from the fit results of the spectra using the software PyMca¹⁶. Since *in situ* measurements are made in the atmosphere, the X-ray energy of the elements with a low mass, below the mass of K, is attenuated. These elements are detected but cannot be considered in the semi-quantification of the data because of the uncertainty of X-ray attenuation.

The chemical concentrations of eleven oxides have been determined on nine figures (Table2) (from one to five measurements per figure). The concentration for each element present in the paint has been evaluated with PyMca in such a way that the contribution in concentration of the substrate detected through the paint layer stays the same. This semi-quantification related to Ca seems to provide a fair comparison between the set of studied representations. Before this, the substrate had been well-characterised, but the subtraction of its contribution proved to be incorrect because of the significant and unquantified bias related to the uncontrolled X-ray incidence and detection angles. This is due to the non-planarity of the wall and plays an important role in the varying fluorescence intensity, being the main experimental uncertainty of the measurement. The calculation of the concentration for each element of the paint was therefore performed without subtracting the signal of the support.

Owing to the acquisition of a large number of values, the use of a principal components analysis (PCA) procedure for their interpretation seemed advised¹⁷.

This statistical treatment has been performed on the determined elemental concentrations, reported in the Table2, by means of the ade4 package implemented in the R environment¹⁸.

Results and discussion

Previous SEM-EDX results

Initial characterisation of a set of samples representative of the colours (black, red, yellow and purple) found at La Garma was the focus of a previous study. This was carried out by SEM-EDX analyses, and provided both morphological and chemical information for each colour.

The black colour has been divided into two types: type 1 composed of charcoal and type 2, composed of manganese oxides. The latter has been attributed to two different oxides according to their chemical composition. For the red colour, one type of iron oxide has been identified as hematite. However, three different types of hematite have been identified, depending on crystal size and morphology. They are labelled as Hp0.3, Hb0.1 and Hp5, consisting of respectively: clay-bearing platelets with sizes ranging from 0.3 to 0.5 μm , spherical grains ranging from 0.1 to 0.2 μm and platelets ranging from 1 to 5 μm .

The two others colours, yellow and purple, are less common. They correspond to mixtures of iron oxide and aluminosilicate minerals. Goethite has been identified as the iron oxide in yellow samples, while hematite with small amount of manganese produces the purple colour.

Their distribution inside the cave is not arbitrary and suggests the use of specific paint pots that indicate the existence of different artistic phases in the overall composition. This is especially notable in the case of the red pigments, for which the morphological structure of hematite varied by the area in which the pigment was applied.

Rock art reference	pXRF points reference	K ₂ O (% oxide)	σ	CaO (% oxide)	σ	TiO ₂ (% oxide)	σ	MnO ₂ (% oxide)	σ	Fe ₂ O ₃ (% oxide)	σ	NiO (% oxide)	σ	CuO (% oxide)	σ	ZnO (% oxide)	σ	As ₂ O ₃ (% oxide)	σ	SiO ₂ (% oxide)	σ	BaO (% oxide)	σ
Stalagmitic columns	AP_LG3	0.221		55.219		0.099		0.027		2.109		0.002		0.012		0.032		0.004		0.088		-	
	AP_LG5	0.448	± 0.122	55.303	± 0.382	0.122	± 0.031	0.026	± 0.010	2.049	± 0.296	0.001	± 0.001	0.015	± 0.003	0.032	± 0.005	0.003	± 0.001	0.068	± 0.025	-	
	AP_LG7	0.257		55.918		0.061		0.043		1.569		0.001		0.008		0.024		0.006		0.038		-	
Horse/IV-11	AP_LG14	0.023		56.310		0.014		0.023		0.894		0.006		0.023		0.069		0.021		0.393		-	
	AP_LG15	0.069	± 0.073	54.421	± 1.305	0.024	± 0.009	0.017	± 0.004	0.965	± 0.125	0.005	± 0.001	0.019	± 0.005	0.045	± 0.015	0.012	± 0.009	0.260	± 0.102	-	
	AP_LG16	0.165		56.925		0.033		0.025		0.722		0.004		0.014		0.041		0.003		0.192		-	
Quadruped/IV-9	AP_LG13	0.267		56.771		0.065		0.042		2.191		0.002		0.014		0.036		0.006		0.154		-	
	AP_LG18	0.015	± 0.178	57.513	± 0.524	0.032	± 0.023	0.042	-	0.762	± 1.010	0.001	± 0.001	0.015	± 0.001	0.040	± 0.002	0.015	± 0.006	0.277	± 0.087	-	
	AP_LG20	0.038		55.918		0.014		0.011		0.860		0.001		0.015		0.042		0.012		0.293		-	
Aurochs/IV-6	AP_LG21	0.055	± 0.049	56.268	± 1.581	0.027	± 0.007	0.019	± 0.007	0.482	± 0.213	0.001	-	0.011	± 0.003	0.024	± 0.009	0.001	± 0.006	0.062	± 0.011	-	
	AP_LG22	0.130		53.372		0.022		0.024		0.838		0.001		0.010		0.028		0.006		0.078		-	
	AP_LG25	0.062		57.289		0.031		0.018		0.240		0.008		0.016		0.039		0.014		0.391		-	
Megabeeros/IV-7	AP_LG26	0.044		55.051		0.042		0.008		0.349		0.001		0.012		0.034		0.010		0.245		-	
	AP_LG27	0.411	± 0.202	56.660	± 0.819	0.044	± 0.007	0.015	± 0.005	0.598	± 0.197	0.003	± 0.003	0.011	± 0.002	0.027	± 0.006	0.005	± 0.004	0.082	± 0.132	-	
	AP_LG28	0.493		56.380		0.039		0.016		0.580		0.003		0.013		0.031		0.006		0.193		-	
	AP_LG29	0.238		56.198		0.050		0.022		0.722		-		0.011		0.025		0.005		0.069		-	
	AP_LG11	0.241		56.827		0.001		0.006		1.627		0.020	± 0.010	0.127		0.251		0.057		2.151		-	
Quadruped/IV-8	AP_LG31	0.235	± 0.102	56.897	± 1.047	0.042	± 0.026	0.016	± 0.005	2.079	± 0.540	-	-	0.021	± 0.003	0.048	± 0.005	0.013	± 0.006	0.357	± 0.036	-	
	AP_LG32	0.061		55.051		0.048		0.014		1.003		0.001		0.017		0.041		0.004		0.409		-	
	AP_LG50	0.097	± 0.039	55.974	± 0.574	0.025	± 0.002	0.025	± 0.007	0.678	± 0.005	0.004	± 0.001	0.018	± 0.005	0.032	± 0.005	0.007	± 0.001	0.013	± 0.037	-	
Mask/IV-12b	AP_LG36	0.052	± 0.029	56.268	± 0.679	0.069	± 0.030	0.406	± 0.107	0.792	± 0.254	0.002	± 0.002	0.017	± 0.006	0.036	± 0.007	0.011	± 0.003	0.133	± 0.038	0.005	± 0.030
	AP_LG44	0.038		57.429		0.029		0.308		0.259		0.002		0.023		0.041		0.010		0.131		0.022	
	AP_LG45	0.010	± 0.029	57.443	± 0.679	0.009	± 0.030	0.449	± 0.107	0.275	± 0.254	0.006	± 0.002	0.020	± 0.006	0.031	± 0.007	0.007	± 0.003	0.074	± 0.038	0.038	± 0.030
The animal/IV-20	AP_LG47	0.041		56.254		0.002		0.567		0.325		0.005		0.010		0.024		0.005		0.061		0.076	

Table 2. Semi-quantitative evaluation of the concentration of pXRF exploitable data using PyMca. The σ value is bigger for some oxides than the measured value, due to the non-planarity of the wall and to the different pigmented density of a paint layer. Relative uncertainties are determined according to the analysis each day of standards before and after the set of measurements and are 10% approx.

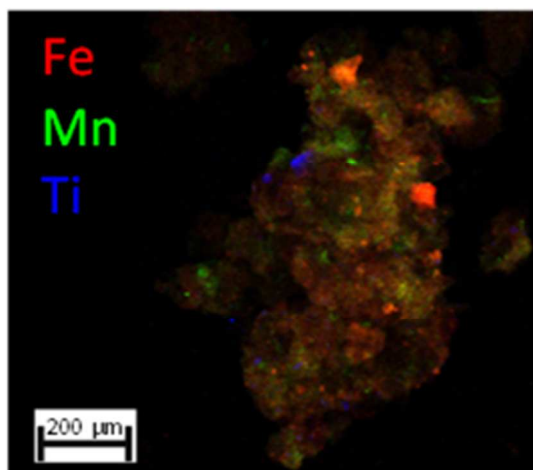


Fig4: Composition of elemental distribution images Fe (red), Mn (green) and Ti (blue), showing the heterogeneity of a selected sample.

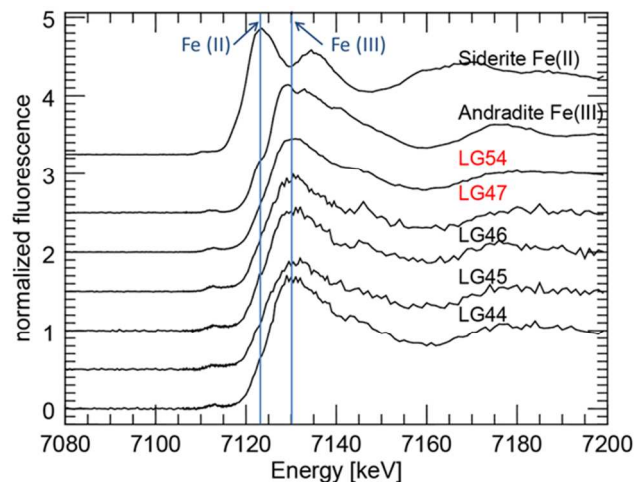


Fig5: The example of XANES profiles extracted from selected samples and two reference compounds. The colours of the sample represent the coloration of the paint samples.

Synchrotron μ XRF/ μ XANES results

Twenty six of the 56 micro-samples studied by SEM-EDX were investigated with μ XRF and μ XANES imaging.

The μ XRF mapping of the samples has revealed a high heterogeneity of the elemental distribution within some of the pigments, as it is exemplary shown in Fig4.

The comparison of μ XANES spectra of the archaeological samples with those acquired for the reference compounds permitted the identification of Fe^{3+} as the predominant oxidation state of iron (Fig5).

However, exact spectrum evaluation according to the procedure for an identification of the chemical species, as described by Wilke *et al.*¹³ was not found possible because of the low signal to noise ratio. This is a result of the reduced time available for the XANES experiments.

Towards a non-invasive analytical strategy by pXRF

Portable XRF analyses have been performed on the paint layer and simultaneously on the underlying rock surface close to the pigment to enable distinguish between the elements characteristic of the pigments from those derived from the painted surface. The effect of the substrate on the paint layer spectrum makes the identification of the chemical components of the pigments difficult. However, main characteristic elements can still be observed on the paint layer spectrum. For example, the spectrum of a red paint layer is shown (Fig6), where Fe, Ti and K can be identified as the main constituents of the pigment.

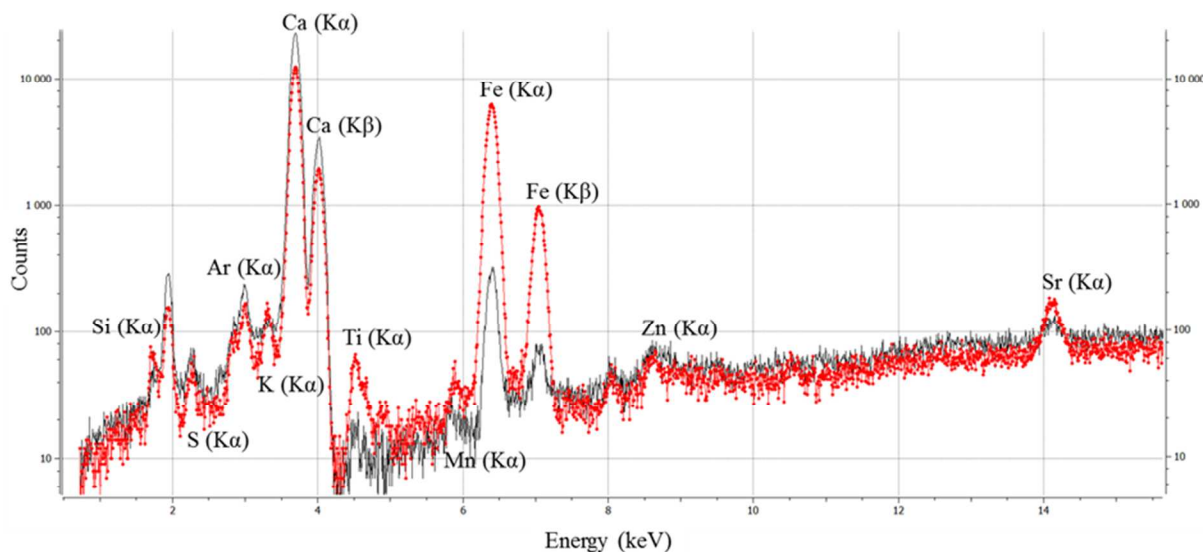


Fig6: XRF spectra from an iron oxide based paint layer (red spectrum) and from the substrate (black spectrum).

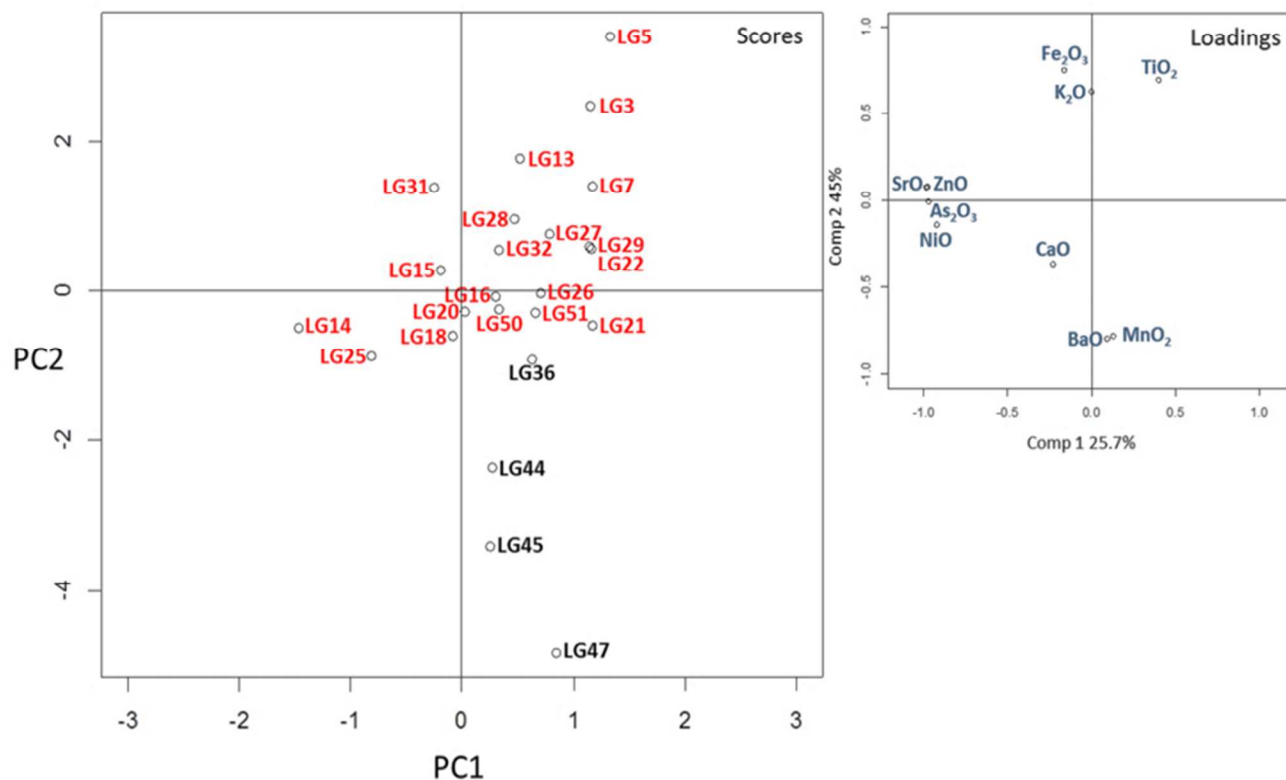


Fig7: Score plot (PC1 vs. PC2) of black representation (black points) and red representation (red points) summarized in the Table1; and loading plot to specify the main oxides influencing the structuration of the dataset.

Multivariate statistical data analyses

The treatment of the dataset by the PCA procedure allows us to identify data groups in principal component (PC) space. The two first principal components explain 45% and 25.7% of the variance, permitting distinction between the main components of the red and black paint layers (Fig7). Thus, Fe_2O_3 associated with TiO_2 and K_2O contribute strongly to the colour of red paint layers whereas MnO_2 and BaO are characteristic of the black pigments.

The second plot (Fig8) is related to the PCA model for the red colour only, and is comprised of data obtained for seven different decorative elements in different areas of the cave. The two first principal components explain 52.5% and 20.5% of the variance. Two groups can be distinguished in the score plot. The first one corresponds to the pigments of five prehistoric drawings located on the same panel (aurochs *IV-6*, megaloceros *IV-7*, quadrupeds (*Ibex or Deer*) *IV-8* and *IV-9*, and horse *IV-11*) and the stain of red matter below the indeterminate animal *IV-20*, in zone IV of the Lower Gallery. The second group is related to the deposit of colorant on stalagmitic columns in the Intermediate Gallery. The main oxide responsible for this second group is Fe_2O_3 . It can be explained by the fact that the pigment of these columns seems to have a higher pigment density than the ornament panel of the zone IV. Moreover, the strongest influence of the substrate contribution (CaO) in the

formation of the Lower Gallery group is clearly visible in this score plot, revealing less densely-pigmented paint layers. These observations provide clear evidence of the impact of pigment density on paint layers.

Potential of a combined data interpretation

The decorated panel of the southern part of zone IV, which includes five red animal representations, is a unique and interesting one, in part because two successive phases of decoration can be distinguished. This is based on the superposition of the figures and the types of paint (different line width and colour of the paint layers are observed): the earlier phase includes the aurochs representation *IV-6* and the quadrupeds *IV-8* and *IV-9*, whereas the later one includes the horse *IV-11* and the megaloceros *IV-7*.

Two different types of hematite constituting the red pigments used to draw these distinct sets of representations have been identified by SEM-EDX. The Hp5 (1-5 μm platelets) hematite species has been identified in the case of the quadruped *IV-9*, the horse *IV-11* and the megaloceros *IV-7*, while the aurochs *IV-6* revealed the use of a different hematite types, the Hb0.5 (0.5 μm spherical grains). Regarding pXRF analyses, no significant differences between the chemical compositions of the red paint layers of all the representations of this panel have been revealed. Neither the chemical composition of these

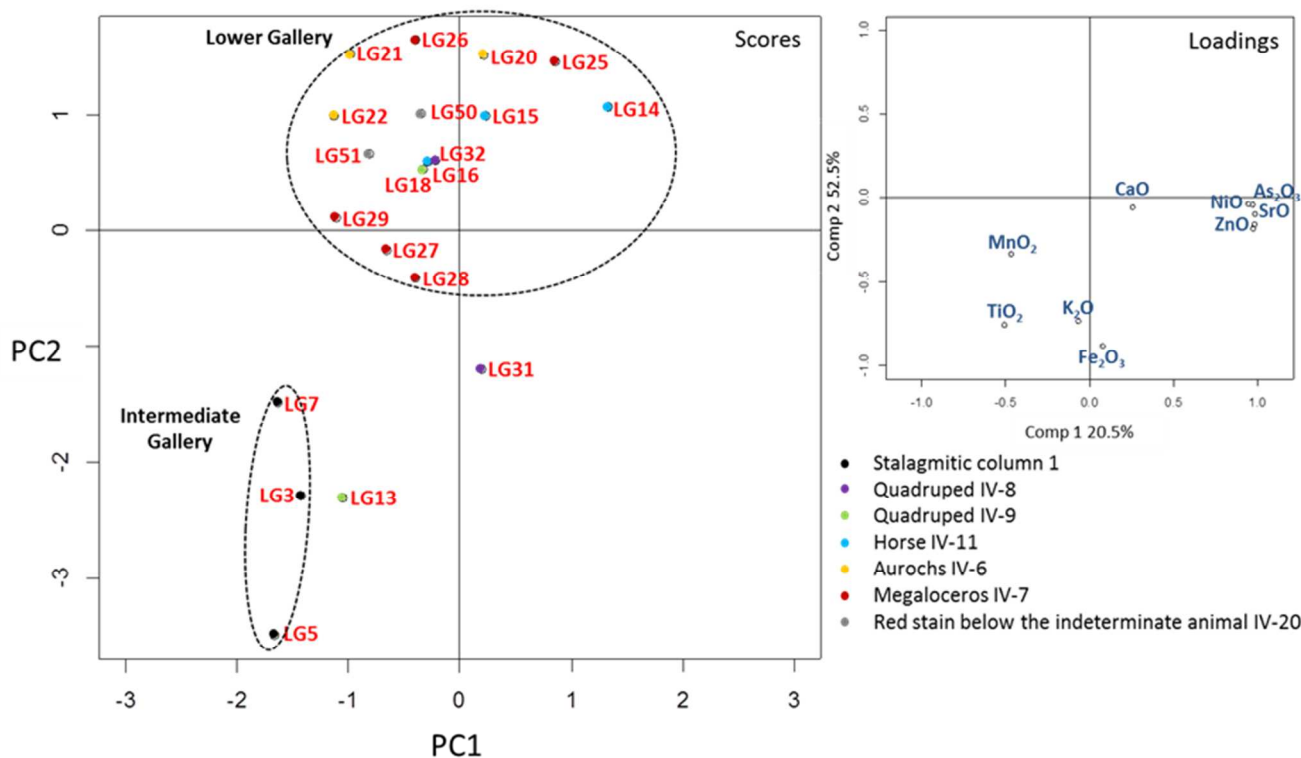


Fig8: Score plot (PC1 vs. PC2) of the red rock art analysed by XRF in the Intermediate Gallery (stalagmitic column 1) and in the Lower Gallery (aurochs IV-6, megaloceros IV-7, quadrupeds IV-8 and IV-9, horse IV-11 and the red stain below the indeterminate animal IV-20); and loading plot to specify the main oxides influencing the structuration of the dataset.

drawings nor the difference between the hematite types could bring new insight to support the stylistic observations and explain the technical difference between the drawings.

Multivariate analyses of the pXRF data did not allow any further discrimination for this panel. However, applied to the red rock art at a widest scale of the cave, the multivariate analysis permitted the identification of two groups, one particular to the Intermediate Gallery and the other to the Lower Gallery. According to the loadings plot, these groups seem to be linked to physical properties (such as grain morphology) of the paint layers rather than to their chemical composition. The SEM-EDX results supplement the former observations. The group of the Intermediate Gallery, corresponding to the LG30 and LG31 samples, is associated to one particular hematite type, Hb0.1 (0.1-0.2 μm spherical grains). The small size of the particles of this hematite type could contribute to the intensity and the high coverage power of these paint layers revealed by the PCA analysis. In contrast, the decorated panel in the Lower Gallery, included in the second group, is related to the LG2, LG5 and LG33 samples identified as Hp5 (1-5 μm platelets). The larger size of the particles of this hematite type could explain the lower intensity and coverage power of the paint layers. The notable differences between these two groups might be linked to different methods of preparation of the paint palette, with different types of hematite mixed (or not) with binders. A higher pigment-density in the paint layer could also explain the distinction between these two

groups. This would indicate different methods of applying paint by prehistoric artists. These methods are directly linked to the surface state of the wall and its geological and physicochemical nature.

To confirm these observations on the preparation of the prehistoric palette and its mode of application, *in situ* analysis of a higher number of representations must be made.

Conclusions and perspectives

This study of the rock art of La Garma has demonstrated the success of a combined approach, relying on the use of synchrotron, laboratory and portable X-ray analyses. The use of one method alone would not provide sufficient new insights into the pigments and therefore more detailed insights into the spatial, stylistic and temporal relationships between the prehistoric representations. However, the combined approach enabled us to distinguish unique paint layers based on their physical properties.

Although the full potential of micro-XANES could not be exploited, the synchrotron X-ray analyses have demonstrated the potential of the method to characterise such heterogeneous prehistoric paint samples and to differentiate between paint layers on the microscopic scale.

In parallel, the XRF evaluation procedure using multivariate statistical analyses has proven to be effective in such studies under difficult on-site conditions. It did not enable a

discrimination of the pigments in terms of their chemical composition due to the inhomogeneous measurement conditions (wall geometry, uncontrolled X-ray incidence and detection angles between the wall and the spectrometer) and the varying contribution from the wall support in the spectra. However, the application of multivariate statistical methods such as PCA in the treatment of pXRF data has shown that a grouping of pigments used to produce different prehistoric figures is possible. These differences are likely related to other non-chemical paint properties such as intensity of the colorant or paint-layer density. These properties are the record of artistic practices of the prehistoric artists, such as methods of paint preparation or the application techniques employed. This study showed that *in situ* results can be used to differentiate prehistoric paint layers by their physical properties. The next phase of this research will be a systematic on-site study of La Garma rock art by portable and non-invasive methods, which can be implemented while preserving the integrity of its prehistoric representations. Further spatially-resolved synchrotron X-ray analyses will be performed for a more precise chemical differentiation of the prehistoric paints.

Acknowledgements

The German Electron Synchrotron (DESY) is acknowledged for having provided beam time at the P06 beamline of PETRA III. Gerald Falkenberg is thanked for the support of this project. Max Wilke is thanked for providing the Fe XANES reference samples.

The authors also acknowledge the support of the LAMS for providing the portable XRF spectrometer as well as the Region Ile de France that provided a PhD grant to Marine Gay at the doctoral school (ED388) of UPMC through the DIM Analytics programme. Africa Pitarch Marti is thanked for her help during the pXRF measurements at La Garma cave. Thank to Claire Heckel of the University of New York for her careful rereading.

Notes and references

^a Sorbonne Universités, Université Paris 6, Laboratoire d'Archéologie Moléculaire et Structurale, UMR 8220 CNRS – Université Pierre et Marie Curie, 4 place Jussieu, 75005 Paris, France.

^b Deutsches Elektronen-Synchrotron DESY, Notkestrasse 85, D-22607 Hamburg, Germany.

^c Centre de Recherche et de Restauration des Musées de France, UMR 8247, Palais du Louvre, 14 quai François-Mitterrand, 75001 Paris, France.

^d Instituto Internacional de Investigaciones Prehistóricas de Cantabria, Universidad de Cantabria, av. de los Castros s/n, 39005 Santander, Spain.

^{*} Rathgen-Forschungslabor, Staatliche Museen zu Berlin-Stiftung Preußischer Kulturbesitz, Schloßstraße 1a, 14059 Berlin, Germany.

1 P. Arias, E. Laval, M. Menu, C. González Sainz and R. Ontañón. *L'anthropologie*, 2011, **115**, 425-445.

2 R. Ontañón. *L'anthropologie*, 2003, **107**, 333-363.

3 P. Arias and R. Ontañón. *Caves in Context: the cultural significance of caves and rockshelters in Europe*, eds. K.A. Bergsvik and R. Skeates, Oxbow, Oxford, 2012, 101-117.

4 P. Arias, R. Ontañón, E. Álvarez Fernández, M. Cueto, M. Elorza, C. García-Moncó, A. Güth, M.J. Iriarte, L.C. Teira and D. Zurro. *Site-internal spatial organization of hunter-gatherer societies: case studies from the European Palaeolithic and Mesolithic*, eds. S. Gaudzinski-Windheuser, O. Jöris, M. Sensburg, M. Street and E. Turner, Verlag des Römisch-Germanischen Zentralmuseums, Mainz, 2011, 31-51.

5 C. González Sainz. *Arte prehistórico desde los inicios del s. XXI. Primer Symposium Internacional de Arte Prehistórico de Ribadesella*, eds. R.de Balbín y P. Bueno, Asociación Cultural Amigos de Ribadesella, Ribadesella. 2003, 201-222.

6 E. Chalmin, C. Vignaud, H. Salomon, F. Farges, J. Susini and M. Menu. *Appl. Phys. A*, 2006, **83**, 213-218.

7 C. Vignaud, H. Salomon, E. Chalmin, J.-M. Geneste and M. Menu. *L'anthropologie*, 2006, **110**, 482-499.

8 J. de Sanoit, D. Chambellan and F. Plassard. *ArcheoSciences*, 2005, **29**, 61-68.

9 M.J. Nuevo, A. Martín Sánchez, C. Oliveira and J. de Oliveira. *X-Ray Spectrom*, 2012, **41**, 1-5.

10 M. Olivares, K. Castro, M.S. Corchón, D. Gárate, X. Murelaga, A. Sarmiento and N. Etxebarria. *J. Archaeol. Sci.*, 2013, **40**, 1354-1360.

11 L. Beck, H. Rousselière, J. Castaing, A. Duran, M. Lebon, B. Moignard and F. Plassard. *Talanta*, 2014, **129**, 459-464.

12 M. West, A.T. Ellis, P.J. Potts, C. Strelis, C. Vanhoof, D. Wegrzynek and P. Wobrauschek. *J. Anal. At. Spectrom.*, 2009, **24**, 1289-1326.

13 M. Wilke, F. Farges, P.E. Petit, G.E. Brown Jr. and Fr. Martin. *Am. Mineral*, 2001, **86**, 714-730.

14 C. G. Ryan, D. P. Siddons, R. Kirkham, Z. Y. Li, M. D. de Jonge, D. J. Paterson, A. Kuczewski, D. L. Howard, P. A. Dunn, G. Falkenberg, U. Boesenberg, G. D. Geronimo, L. A. Fisher, A. Halfpenny, M. J. Lintern, E. Lombi, K. A. Dyl, M. Jensen, G. F. Moorhead, J. S. Cleverley, R. M. Hough, B. Godel, S. J. Barnes, S. A. James, K. M. Spiers, M. Alfeld, G. Wellenreuther, Z. Vukmanovic and S. Borg. *J. Phys.: Conf. Ser.*, 2014, **499**, 012002.

15 C. Ryan, B. Etschmann, S. Vogt, J. Maser, C. Harland, E. van Achterbergh and D. Legnini. *Nucl. Instrum. Methods Phys. Res., Sect. B*, 2005, **231**, 183-188.

16 V.A. Solé, E. Papillon, M. Cotte, P. Walter and J. Susini. *Spectrochim. Acta, Part B*, 2007, **62**, 63-68.

17 M.J. Baxter and I.C. Freestone. *Archaeometry*, 2006, **48**, 3, 511-531.

18 D. Chessel, A.B. Dufour and J. Thioulouse. *R News*, 2004, **4**, 5-10.

1
2
3
4
5
6
7
8
9
10
11
12
13
14
15
16
17
18
19
20
21
22
23
24
25
26
27
28
29
30
31
32
33
34
35
36
37
38
39
40
41
42
43
44
45
46
47
48
49
50
51
52
53
54
55
56
57
58
59
60

This rock art study of La Garma provides new and original insights into the characterisation of the prehistoric paint palette.